Volume 1 | Number 1 | Jan 2013 | Pages 1–100

Dalton Transactions

An international journal of inorganic chemistry
www.rsc.org/dalton

ROYAL SOCIETY OF CHEMISTRY

ROYAL SOCIETY OF CHEMISTRY

www.rsc.org/dalton

Fabrication of Ultrathin CoMoO₄ Nanosheet Modified with Chitosan and their Improved Performance in Energy Storage Device

Ramya Ramkumar and Manickam Minakshi*

Energy, School of Engineering and Information Technology, Murdoch University, WA 6150,

Australia

Abstract

Ultrathin nanosheet-assembled cobalt molybdate (CoMoO₄) owing to the mesoporous morphology was synthesized by urea-assisted solution combustion route at a temperature of 400 °C. The as-prepared CoMoO₄ was modified using chitosan cross-linked with glutaraldehyde (glu) and employed as a cathode material in an aqueous hybrid capacitor. The physical and electrochemical behaviour of the CoMoO₄ modified with chitosan and the as-prepared (chitosan free) CoMoO₄ has been compared and discussed. The modified CoMoO₄ exhibited excellent electrochemical performance with a specific capacitance of 135 F/g at 0.6 A/g and an energy density of 31 Wh/Kg. It also exhibited good cycling stability with high coulombic efficiency over 2000 cycles retaining a specific capacitance of 81 F/g at 3 A/g, comparatively much better than those of nanostructured chitosan free CoMoO₄ which yielded 17 F/g. The results indicated that the chitosan gel strongly adheres to the molybdate moiety of CoMoO₄ and increased the capacitance four-fold compared to the chitosan free material. The modified CoMoO₄ electrode shows potential for a high performance, environmental friendly and low-cost energy storage device.

Keywords: Cobalt molybdate, chitosan, activated carbon, hybrid device, aqueous.

*E: *R.Ramkumar@murdoch.edu.au ; minakshi@murdoch.edu.au*
T: 61 (8) 9360 2017

1

1. Introduction

The available renewable energy sources provide only intermittent energy. Thus, energy storage systems are required for allowing energy to be stored and used on demand. Energy storage in rechargeable batteries and supercapacitors is the most promising prospect for ensuring consistent energy supply, therefore allowing greater penetration of renewable energy into the electricity grid. In this context, electrochemical energy storage has been the main topic of interest in the recent years [1-7]. The salient features of electrochemical energy storage include low maintenance, excellent efficiency, cycling stability and environmental friendly. Hybrid devices have attracted a considerable amount of interest in future energy storage applications [4, 8-13] while delivering high energy density with comparable power density [11]. Hybrid devices such as asymmetric capacitors bridge the gap between electrochemical double layer capacitors (EDLC) and pseudocapacitors [4]. Conventional electrochemical capacitors store energy using ion adsorption while pseudocapacitors store energy using both ion adsorption and electron transfer processes. A range of candidates can be employed as electrodes for hybrid devices. In continuation to our ongoing work on metal oxides, phosphate and lithium based materials as cathode materials [12-13], in the current work, we have extended our interest to molybdate. Transition metal molybdates, in particular, cobalt molybdate has attracted great interest because of its high redox activity, and excellent catalytic characteristics [14-15]. The anode material can vary from activated carbon, carbon nanotubes to the most expensive graphene but in the current work an inexpensive activated carbon has been used to fabricate the aqueous hybrid capacitor.

Metal molybdates are salts of molybdenum acid with the general formula $MMoO_4$ (where M is divalent cation such as Co, Mn, Ni, Ca, Fe, Cu, or Pb). Metal molybdates are commonly employed as catalysts [16], in energy storage devices [17], as optoelectronic materials [18] and for magnetic applications [19] owing to their unique physical and chemical

2

properties. Recently, cobalt molybdate synthesized via hydrothermal route for supercapacitors has been reported with a specific capacitance, 1558 F/g *vs*. SCE, exhibiting excellent cyclability and storage capability [20-21]. Several other synthetic strategies have been adopted to improve the electrochemical performance of the cobalt molybdate based capacitors [22-25]. Nickel and manganese molybdates have also attracted greater attention as electrode materials for hybrid devices. A microwave assisted $NiMoO_4$ as an electrode yielded 680 F/g *vs*. Hg/HgO [26]. Another study involving $NiMoO_4$ and $NiCo_2O_4$ as composites yielded a specific capacitance 2474 F/g *vs*. SCE [27]. $MnMoO_4$/graphene hybrid composite yielded a specific capacitance 364 F/g in a three electrode system [28]. In comparison to the hitherto known metal molybdates, $CoMoO_4$ based energy storage devices are preferred because it is scalable, has high redox potential and non-toxic with improved electrochemical properties [29]. The $CoMoO_4$ reported in the literature [20-25] are predominantly oriented to single electrode study and the available reports on the supercapacitive properties of $CoMoO_4$ as a device (*Activated carbon vs. CoMoO₄*) are scant.

Cobalt molybdate ($CoMoO_4$) can be prepared by various synthetic conditions leading to diverse chemical and morphological variations. The cobalt molybdate synthesized at low temperature yields an alpha structure (α-$CoMoO_4$), while the β phase appears at temperatures above the range 400° – 650 °C [24, 30-31]. It is also reported [32] that β-$CoMoO_4$ has disordered structure with random distribution of Co and Mo atoms in oxygen interstitials and may not be stable. Hence, α-$CoMoO_4$ has been synthesized at 400 °C via solution combustion synthesis using urea as a fuel to obtain nanostructured porous flaky particles possessing good surface area and surface to volume ratio. To improve the supercapacitive behavior of the currently available $CoMoO_4$ material, a unique biopolymer approach has been proposed in

3

this study to enhance the kinetics of ion and electron transport leading to long durability with high discharge/charge rates.

Chitosan is a biopolymer produced by N-deacetylation of chitin, the most abundant natural polymer, along with cellulose. This new biopolymer approach has been adapted to a $CoMoO_4$ electrode, as the molybdates strongly adheres to the polymer network [33]. Chitosan, a deacetylated product of chitin from the exoskeleton of crustaceans is a polysaccharide with two basic repeating units, the GlucNAc(N-acetyl glucosamine) and GlucN(glucosamine) [34]. Chitosan has been used in several applications ranging from green chemistry, biomedical, pharmaceutical and agriculture due to its wide range of physicochemical properties. It is employed in removal of heavy metals from waste water, because of its chelating properties with transition metal ions [35-36]. $LiClO_4$ doped chitosan has also been employed as polymer gel electrolyte [37] and as binder [38] for supercapacitor applications [39]. Electrodeposited MnO_2-chitosan nanocomposite employed as a supercapacitor device yields a specific capacitance 424 F/g *vs*. Ag/AgCl [40]. A recent study by Pandiselvi et al on supercapacitor properties of a ZnO, polyaniline and chitosan composite yielded a specific capacitance 587 F/g *vs*. SCE [41]. To the best of our knowledge, no work on biopolymer chitosan has been reported in metal molybdates and employed as an active electrode for energy storage applications. Here, we have fabricated a hybrid device employing chitosan-free $CoMoO_4$ and $CoMoO_4$ with chitosan *versus* activated carbon (AC) in aqueous sodium hydroxide electrolyte. A preliminary work on $CoMoO_4$ that has been published by us earlier [42] in LiOH electrolyte showing a specific capacitance that is way lower than that of the currently reported modified $CoMoO_4$ in NaOH electrolyte. The objective of this work is to attain improved capacitance through the use of inexpensive biopolymer chitosan (gelated) in the molybdate material.

4

2. Experimental

2.1 Material preparation

Cobalt molybdate (α-CoMoO$_4$) was synthesized by a solution combustion synthesis. The synthesis procedures followed for chitosan-free CoMoO$_4$ are identical to that of our earlier reported work [42]. Urea played a dual role, as complexing agent for the metal molybdate in the solution and as a fuel for the synthesis of nanoscale cobalt molybdate powder. For modified CoMoO$_4$, chitosan solution was prepared initially with the procedures identical to that of Iglesias et al [43] then reacted with glutaraldehyde (glu) to form the resultant gel, to which CoMoO$_4$ powder was added. Chitosan was cross-linked with different amounts of glu and the best concentration was chosen for preparing the polymeric structure "modified CoMoO$_4$". The precursors and the low molecular weight chitosan powder with 75-85% degree of deacetylation were obtained from Sigma Aldrich (USA). Glutaraldehyde (glu) 25% solution in water was obtained from Sigma Aldrich (USA). Acetic acid was purchased from Sigma. The optimal mass ratio between molybdate and activated carbon was determined to be 1.6 for the fabricated hybrid capacitor. The mass balance was calculated using the following equation (1)

$$m+ /m- = (C_- * \Delta E_-) \ / (C_+ * \Delta E_+) \quad (1)$$

where C is the specific capacitance; ΔE is the potential range for the charge / discharge processes. The mass of the positive and negative electrode material was 2.0 and 3.2 mg, respectively.

2.2 Physical characterization

The as-prepared (chitosan-free) CoMoO$_4$ and modified CoMoO$_4$ samples were characterized by physical techniques. Phase identification was carried out by powder X-ray diffraction (XRD) using Siemens D500 X-ray diffractometer 5635 with Cu Kα source at a scan speed of

1° /min. The voltage and current were 40 kV and current 28 mA, respectively. Attenuated total reflectance- Fourier transform infrared (ATR-FTIR) studies were carried out with a Bruker IFS 125/HR spectrometer. To investigate the microstructure of the prepared samples, high magnification Zeiss Neon 40EsB focussed ion beam-scanning electron microscope (FIB-SEM) instrument was utilized. The surface morphology of the samples was characterized by transmission electron microscopy (TEM), with energy dispersive X-ray detector (EDS) using a JEOL 2010F TEM operated at 200 kV. TEM specimens were prepared by grinding a small amount of powder sample in ethanol and dispersing on a holey carbon support grid.

2.3 Electrochemical characterization

The working electrode consists of active material $CoMoO_4$ or AC (85 wt %), carbon black (10 wt %) and polyvinylidene fluoride (PVDF) (5 wt %). The composites were suspended in an agate mortar containing 0.3 mL of N-methyl-2-pyrrolidinone (NMP) to form slurry. A total of 10 μL of slurry was coated on a graphite sheet (geometric surface area of 1 cm^2) and then dried at 60 ºC for an hour. An aqueous solution of 2 M NaOH was employed as the electrolyte for all electrochemical measurements. For the three-electrode tests, a platinum wire of 10 cm in length and 1 mm in diameter and a mercury-mercuric oxide (Hg/HgO) served as the counter and reference electrode, respectively. The hybrid capacitor was constructed with $CoMoO_4$ or modified $CoMoO_4$ as a positive electrode and activated carbon as a negative electrode. The electrochemical measurements were carried out using BioLogic VSP-300 instrument. For cyclic voltammetric (CV) experiments, the working electrode was cycled between 0 and 1.4 V at a range of scan rates between 5 and 100 mV/s. Galvanostatic charge-discharge studies were carried out at various current densities ranging between 1 and 10 mA/cm^2. The cut-off charge and discharge voltages were 1.6 and 0.2 V. Electrochemical

impedance spectroscopy was carried out with amplitude of 10 mV over a frequency range 10

mHz to 200 kHz at open circuit potential.

3. Results and Discussion

3.1 Structural characterization – XRD and FTIR studies of $CoMoO_4$

The X-ray diffraction (XRD) pattern observed for as-prepared $CoMoO_4$ at 400° C in

Fig. 1A reproduced well the peak positions of the patterns reported in the literature [44] and

powder diffraction file (PDF), card nos. 25-1434 and 21-0868. This confirms that the chosen

solution combustion method for synthesis is apt and led to the formation of a pure phase of

$CoMoO_4$. A well-resolved pattern with broadening of peaks in Fig. 1A suggests that the

synthesized powder is nanocrystalline. Cobalt molybdate ($CoMoO_4$) exists in two different

phases, usually designated as α and β. On heating the α-phase, a phase change occurs above

650° C which appears to be complete at about 750° C, forming β-phase [32]. Both the phases

crystallise in a monoclinic structure with a space group of C2/m, while the observed

diffraction peaks in Fig. 1A are in good agreement with that of α-$CoMoO_4$. The X-ray

diffraction pattern for the $CoMoO_4$ modified with chitosan (Fig. 1B) showed a change in

crystalline structure in the presence of polymer i.e. few $CoMoO_4$ weak diffraction peaks have

been seen indicating an amorphous nature with nanocrystalline size. This could be attributed

to the hydroxyl ions from hydrated glutaraldehyde, amino and hydrogen bond from chitosan,

cross-linking with the $CoMoO_4$ particles resulting in the polymeric structure [45], a pre-

requisite for capacitors in enhancing the adsorption/desorption processes. This conceptual is

in agreement with the characteristic diffractogram of the chitosan with the concentration of

glutaraldehyde showing amorphous nature [46]. This may be correlated to the SEM and TEM

observations in the next section showing few differences in the structure of different

materials.

The infrared spectra of $CoMoO_4$ samples (a) as – prepared (chitosan free), (b) chitosan dissolved in acetic acid, and (c) chitosan dissolved in acetic acid and reacted with glutaraldehyde to form the cross-linked gel, to which $CoMoO_4$ powder was added and termed as "$CoMoO_4$ modified with chitosan" are shown in Figure 1C. In comparison, the FTIR spectra of a, b and c indicate that the modified $CoMoO_4$ samples are different from that of as-prepared $CoMoO_4$ samples. The typical stretching vibrations related to the chitosan moiety are assigned as follows: 1710, 1555, 1410, 1289, 1235, 1053, 1010, 885 cm^{-1} (C=O in acetamide group, N−H in amino group, O−H, C−H symmetric stretch in the ring, C−H structure in acetamide). The $CoMoO_4$ exhibits an O−H vibration corresponding to the water molecule physically adsorbed on the $CoMoO_4$ particles in the structure and the stretching vibration of Mo−O−Mo at 650 cm^{-1}. The modified $CoMoO_4$ with chitosan exhibits all the frequencies except that the amide band N−H decreased in intensity, C−O stretching vibration is shifted to 1680 cm^{-1} and the Mo-O-Mo peak slightly shifted to the lower wavenumber, indicating the affinity with chitosan moiety. The result from this study is consistent with the earlier reported work on chitosan [47-48] demonstrating a difference in profile between chitosan-free and modified chitosan.

X-ray diffraction and infrared studies supports the concept that the as-prepared $CoMoO_4$ is crystalline and chitosan cross-linked with glutaraldehyde (glu) sample is quite distinct. To reveal detailed information, microstructure and its morphological aspects have been studied through FIB-SEM and TEM imaging.

3.2 Physical characterization – FIB-SEM and TEM studies of $CoMoO_4$

FIB-SEM images of as-prepared $CoMoO_4$ and $CoMoO_4$ modified with chitosan are shown in Fig. 2. The as-prepared $CoMoO_4$ (Fig. 2A) exhibits well - defined interconnected nanosheets with flaky and mesoporous nature. The modified $CoMoO_4$ with chitosan (Fig. 2B) exhibited

uniform structure, with coagulated surface which can be attributed to the immobilization of CoMoO$_4$ on the glu cross-linked structure of chitosan. The surface morphology in Fig. 2B is not well defined, which may be due to the core CoMoO$_4$ particles being hindered by surface modification of biopolymer chitosan with glu and this has also been verified by EDS analysis shown in Fig. 3.

The transmission electron microscopy images of the as-prepared CoMoO$_4$ and CoMoO$_4$ modified with chitosan are shown in Figs. 3A and C. The CoMoO$_4$ powder can be seen as crystalline having nanosheets with mesoporous morphology. The elemental analysis (Fig. 3B) corresponding to CoMoO$_4$, shows that the particles mainly constitute Co and Mo. The selected area diffraction pattern (SADP) of this region (inset left) showed well defined series of rings (0.26 nm doublet; 0.22 nm broad; 0.11 and 0.10 are very diffuse) which supports the crystallinity of the synthesized powder. The chosen solution combustion synthesis aids in producing nanocrystalline sizes without any particle agglomeration. Nitrate precursor acts as an oxidizer for the fuel during the combustion reaction leaving the final products in nanometer range [49].

On the other hand, TEM images of CoMoO$_4$ modified with chitosan (Fig. 3C) exhibits a different morphology illustrating the presence of CoMoO$_4$ matrix well dispersed in the glu cross-linked chitosan matrix. As shown in Fig. 3C, the length of the flakes decreases and agglomerates with an overall increase in the surface area of the CoMoO$_4$ polymer structure. The high resolution TEM (inset right) shows fringe like patterns which are not well defined indicating that the cross-linked structure is less crystalline than that of the as-prepared CoMoO$_4$. The SADP of the modified material in Fig. 3C (inset left) indicates the appearance of well defined, broad and diffused rings corresponding to 0.21 nm, 0.12 and 0.09 nm which are in agreement with the as-prepared sample. This shows that the modified

$CoMoO_4$ retains the crystal structure of as-prepared $CoMoO_4$ but the surface morphology has been varied, as evidenced from elemental analysis (Fig. 3D). The peaks corresponding to the elements Al and Si have come from the microscope pole piece which is of no interest in study. An interface between the organic chitosan and the metal structure can be inferred from another region of the TEM image (Fig. 3E). This suggests that cross-linking has occurred, which is crucial to enhance the kinetics of ion and electron transport in order to improve the specific capacitance. This verifies that molybdate gelated chitosan has been successfully fabricated to be used as an electrode for capacitor applications.

To examine the elemental composition along with electronic structure with greater sensitivity [50] scanning transmission electron microscopy (STEM) has been used. A raw STEM image for the as-prepared and $CoMoO_4$ modified with chitosan is compared in Figs. 4A and B. The as-prepared $CoMoO_4$ appeared to be quite flaky and aggregated to the centre. The modified sample indicates the presence of nanosheet like assembly with an agglomeration of nanoparticles, forming clusters that were several nanometers in size. The STEM images allow us to thoroughly investigate the composition profiles across the $CoMoO_4$ particles. The intensity profile showing relative amounts of cobalt, molybdenum and oxygen in the modified sample (Fig. 5B) appears to be evenly distributed throughout the section and intact in nature than that of the as-prepared sample shown in Fig. 5A. This further confirms the results of EDS analysis.

3.3 Electrochemical characterization

The electrochemical measurements were carried out using cyclic voltammetry (CV), galvanostatic charge-discharge, and electrochemical impedance spectroscopy (EIS) studies.

3.3.1 Cyclic voltammetry (three – cell configuration) studies of CoMoO$_4$

The working electrode (CoMoO$_4$) was cycled between -0.3 and 0.6 V *vs*. Hg/HgO. On each occasion the potential scan was initiated at -0.3 V, scanning in the anodic direction (oxidation) to 0.6 V and then reversing it back to the starting potential in the cathodic direction (reduction). The typical CV curves for as-prepared and modified CoMoO$_4$ samples obtained at different scanning rate between 5 and 100 mV/s are shown in Fig. 6. While only one ill-defined oxidation (A$_1$ = 0.42 V) and reduction peak (C$_1$ = 0.04 V) is seen for the as-prepared CoMoO$_4$ (Fig. 6A), one well-defined anodic peak (A$_1$ = 0.38 V) and two prominent cathodic peaks (C$_1$ = 0.39 and C$_2$ = 0.14 V) are observed for the modified CoMoO$_4$ (Fig. 6B). These results suggest that the electrochemical process between these two samples is quite different. The observed potential difference between the redox peaks (A$_1$ and C$_1$) for modified CoMoO$_4$ is smaller than the as-prepared CoMoO$_4$, implying that the modified material is more reversible [1]. For the modified CoMoO$_4$, the product formed during the oxidation process (A$_1$) undergoes two separate reduction processes (C$_1$ and C$_2$) during the reverse cathodic scan. The proposed electrochemical reaction of the CoMoO$_4$ during the oxidation and reduction are as follows involving Co^{2+}/Co^{3+} in the CoMoO$_4$ framework [42, 51]:

$$3[Co(OH)_3]^- \longleftrightarrow Co_3O_4 + 4H_2O + OH^- + 2e^- \qquad (2)$$

$$Co_3O_4 + H_2O + OH^- \longleftrightarrow 3CoOOH + e^- \qquad (3)$$

$$CoOOH + OH^- \longleftrightarrow CoO_2 + H_2O + e^- \qquad (4)$$
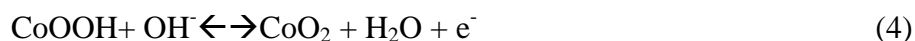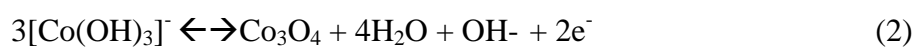
The as-prepared CoMoO$_4$ could be involved in the reversible formation of Co$_3$O$_4$ and CoOOH (Eq. 2 and 3) but the modified CoMoO$_4$ could have extended the redox reaction to the formation of CoO$_2$ (Eq. 2, 3 and 4). As the scanning rate was increased, the area under the peak also increases (in Fig. 6B) that led to the increased peak current. The oxidation (A$_1$) and reduction peaks (C$_1$; C$_2$) are more prominent at higher current rate while retaining the

11

shape for the modified $CoMoO_4$. At higher current rates, the oxidation and reduction peak potentials are getting more positive and negative, respectively. This could be due to the substantial polarization at higher scan rates. As the scan rate increases from 5 to 100 mV/s, the observed peak currents are proportional to the square root of the applied scan rate, which implies the diffusion controlled process. However, the uniform linear increase in current with scan rate is observed only for $CoMoO_4$ modified with chitosan suggesting the fast kinetics of the interfacial faradaic reactions and also the ease of ionic and electronic transport [52]. In contrast, the as-prepared $CoMoO_4$ suggests a sluggish kinetics with marginal increase in current response. The shape of the CV curves and the presence of strong redox peaks indicate that the reactions involved are mainly Faradaic in nature but also exhibits a similarity to the rectangular electrochemical double-layer capacitor (EDLC) behavior (see also Fig. 8b, discussed in the next section) attributed to non-Faradaic process, which collectively increases the specific capacitance of the modified $CoMoO_4$ than the as-prepared material. The chitosan is electrochemically inactive and acts solely as a matrix in the $CoMoO_4$ structure and assist in the penetration of ions freely in and out of the electrode [53] resulting in enhanced capacitive properties. Interestingly, only molybdate ions are very efficient gelating agents for chitosan, we have tried with phosphate species but the gelated material was not found to be suitable for capacitive applications.

3.3.2 Charge-discharge (galvanostatic) studies of $CoMoO_4$ *vs*. Activated Carbon

Since the major objective of this work is to establish whether the synthesized material could be used to develop a hybrid device for energy storage applications, electrochemical (galvanostatic) behavior of $CoMoO_4$ vs. activated carbon has been investigated in 2M NaOH electrolyte. Figure 7 shows the typical charge-discharge characteristics of the $CoMoO_4 \parallel$ AC at various current densities ranging from 1 to 10 mA/cm^2 and the results are tabulated in

Table 1. The device could be reversibly charged and discharged. The shape of the charge curve (Fig. 7A) is characterised by an initial rise in voltage to 0.4 V, followed by a gradual upward-sloping potential profile until 1.2 V and then a plateau like curve until the 1.5 V cut-off voltage. The discharge profile is a mirror image of the charge curve and fully reversible. The results obtained from modified $CoMoO_4$ (Fig. 7B) are much improved compared to the as-prepared $CoMoO_4$ (Fig. 7A). The nature of the charge/discharge curves was symmetrical for the modified $CoMoO_4$ indicating increased coulombic efficiency and low polarization to that of as-prepared $CoMoO_4$. A similar behavior is also observed from CV curves (in Fig. 8) for the $CoMoO_4$ ∥ AC cell examined under potentiostatic conditions at various sweep rates ranging from 5 to 100 mV/s and the results are tabulated in Table 2. The symmetric nature of the CV curves and the reversible current response on voltage sweeps indicate the ideal supercapacitor behaviour for the modified $CoMoO_4$ (Fig. 8b). The specific capacitance values of modified $CoMoO_4$ calculated from the time taken for discharge are 135, 110 and 105 F/g at current densities of 0.6, 1.2 and 6.0 A/g, respectively as shown in figure 7B. The specific capacitance decreased with the increase in current density because of the increased ohmic drop and scarcity of active material at the electrode/electrolyte interface available for the Faradaic reactions. Nevertheless, at a relatively high current density of 6 A/g, the specific capacitance is still retained at 105 F/g which is about three-fold higher than the as-prepared $CoMoO_4$ (30 F/g), indicating the excellent rate capability of the chitosan modified electrode material. The nanosheet with mesoporous structure, having chitosan as metal ion sorption moiety with strong affinity towards molybdate [54], influences the greater diffusion of electrons and ions into the inner regions of the electrode and result in fast electron/ion transport processes.

13

3.3.3 Electrochemical Impedance Spectroscopy (EIS) studies of cycled CoMoO$_4$ *vs*. Activated Carbon

EIS is the most effective and simple tool to investigate the changes occurring at any electrode/electrolyte interface [55]. EIS is performed on the as-prepared and modified CoMoO$_4$ electrodes from 10 mHz to 200 kHz at open circuit potential with an amplitude of 10 mV and the Nyquist plots are displayed in Figure 9. The impedance data was fitted using a Randles circuit. The solution resistance (R$_s$) in the high frequency region for the as-prepared and modified CoMoO$_4$ are 9 Ω and 7 Ω respectively. The charge transfer resistance (R$_{ct}$) for the as-prepared CoMoO$_4$ is 20 Ω and for the modified CoMoO$_4$ is 4 Ω. The low resistance values indicate the high electronic conductivity of the cycled CoMoO$_4$ samples. The low frequency Warburg impedance and diffusional capacitance appeared to be almost the same for both electrodes, with slightly enhanced double-layer capacitance (C$_{dl}$) for the chitosan modified material. The R$_{ct}$ and Warburg values of as-prepared and modified electrode materials before undergoing any electrochemical measurements (not shown) were quite distinct with high resistance. This could be due to the poor electrical conductivity of CoMoO$_4$ with the electrolyte.

3.3.4 Long-term performance test of CoMoO$_4$ *vs*. Activated Carbon

The cyclability of the as-prepared and modified CoMoO$_4$ were evaluated through long term performance tests (2000 charge-discharge cycles) at the chosen constant current density and the results are shown in Figure 10. It can be seen from Table 1 that with increasing current density the specific capacitance gradually decreases as a consequence of lower active redox sites. However, even at a high current density of 3 A/g, the specific capacitance retention was found to be 78% for modified CoMoO$_4$ implying an excellent rate capability of the material. Based on these results, current density of 3 A/g was chosen to perform the cyclability test. The CD curves are shown for the first and last (2000) cycles for both the materials. The

specific capacitance decreases for the as-prepared $CoMoO_4$ initially, but stabilizes after few

cycles yielding 17 F/g while for the modified $CoMoO_4$ the available specific capacitance

increases until 300 cycles and then stabilises over 2000 cycles possessing 81 F/g. The initial

increase in specific capacitance could be due to the wetting effect and then stabilizes and

sustained 2000 cycles (tested until now) reflecting excellent reversibility and follows the

general trend of capacitive materials. The chitosan-glu cross-linking influences the degree of

amorphosity in the composite, decreasing the particle size and promoting the formation of

cluster like particles that yield a larger capacitance (of about 4 times). The improved

performance may also originate from the porous polymer structure that can fully allow the

ions to adsorb/desorb during the reactions.

The energy density and power density can be calculated from the following equations:

$$\text{Energy density } (E) = \frac{1}{2} C_{sp}(\Delta V)^2 \tag{5}$$

$$\text{Power density } (P) = E/T \tag{6}$$

Where C_{sp} is the specific capacitance in F/g, ΔV is the voltage window and T is the discharge

time in seconds (calculated from the charge/discharge curves). Figure 11A shows the energy

density *vs*. current density of $CoMoO_4$ modified with chitosan. A high energy density of 31

Wh/Kg has been obtained at a lower current density of 0.6 A/g but the energy density

decreased to 25 Wh/Kg at 1 A/g and then fairly stabilised for higher current rates suggesting

that the material is superior and suitable for power applications. The reported value of

capacitance in the literature for $CoMoO_4$, $MnMoO_4$, $NiMoO_4$, $MnMoO_4$-$CoMoO_4$, $CoMoO_4$-

MWCNTs, and $CoMoO_4$-$NiMiO_4.H_2O$ are all confined to a single electrode study [17, 24,

26-28, 51, 56-57]. To our knowledge, 81 F/g is the excellent capacitance at a current density

3 A/g never reported for $CoMoO_4$ *vs.* activated carbon cell. Also, the obtained capacity

retention and excellent coulombic efficiency is high compared with that reported for typical

metal oxides A Ragone plot for the modified $CoMoO_4$ is compared with some of the available capacitors in the market and the results are shown in Figure 11B. The asymmetric $CoMoO_4 \| AC$ capacitor delivers an energy density of 31 Wh/Kg at a high power density of 1000 W/Kg. The modified $CoMoO_4$ with chitosan electrode shows excellent performance which is significantly greater than the oxide based and EDLC based supercapacitors shown in the Figure 11B.

4. Conclusions

A biopolymer based cobalt molybdate reported as an electrode for energy storage device is novel with an excellent cycling stability of over 2000 cycles (tested until now) exhibiting 97% coulombic efficiency. Molybdate moiety has been proven to be a potential host for accommodating the chitosan molecule. Interestingly, biopolymer chitosan can adsorb metal ions and this property has enhanced the capacitive behaviour of the modified $CoMoO_4$ electrode. The physical and electrochemical test results indicated that the chitosan gel strongly adheres to the molybdate moiety of $CoMoO_4$ and increased the capacitance (81 F/g) four-fold compared to the chitosan free material (17 F/g). This work paves the way for an alternative energy future by removing global reliance on fossil fuels, replacing them with sustainable Na-based hybrid device. The energy density of the modified $CoMoO_4$ with chitosan is 31 Wh/Kg and the performance is competitive to that of oxide based material available in the market.

Acknowledgements

References

1. M. Minakshi and D. Meyrick, Electrochim. Acta, 101 (2013) 66–70.

2. L. Mai, X. Tian, X. Xu, L. Chang and L. Xu, Chem. Rev., 114 (2014) 11828–11862.

3. B. E. Conway, *Electrochemical Supercapacitors: Scientific Fundamentals and Technological Applications*, Kluwer Academic/Plenum Press, New York, 1999.

4. L. Li, Z. Wu, S. Yuan and X.-B. Zhang, Energy Environ. Sci. 7 (2014) 2101 – 2122.

5. Z. Wu, X.-L. Huang, Z.-L. Wang, J.-J. Xu, H.-G. Wang and X.-B. Zhang, Sci. Rep. 4 (2014) 3669.

6. Z.-L. Wang, D. Xu, J.-J. Xu and X.-B. Zhang, Chem. Soc. Rev. 43 (2014) 7746 – 7786.

7. X. – L. Huang, J. Chai, T. Jiang, Y.-J. Wei, G. Chen and W.-Q. Liu, D. Han, L. Niu, L. Wang and X.-B. Zhang, J. Mater. Chem. 22 (2012) 3404 – 3410.

8. H. Wang, D. Ma, X. Huang, Y. Huang and X. Zhang, Sci. Rep. 2 (2012) 701.

9. R. F. Service, Science, 313 (2006) 902–905.

10. P. Simon and Y. Gogotsi, Nat. Mat., 7 (2008) 845–854.

11. F. Chevallier, C. Clinard, E. Frackowiak, J. N. Rouzaud, F. Beguin, M. Morcrette, and J. M. Tarascon, J. Chem. Phys., 118 (2003) 6038–6045.

12. M. Minakshi, K. Minato and M. Takata, J. Electrochem. Soc., 150 (2003) A1085–A1089.

13. M. Minakshi, P. Singh and D. R. G. Mitchell. J. Electrochem. Soc., 154 (2007) A109–A113.

14. Y. Q. Fan, H. B. Shao, J. M. Wang, L. Liu, J. Q. Zhang and C. N. Cao, Chem. Commun., 47 (2011) 3469–3471.

15. L. M. Madeira, M. F. Portela and C. Mazzocchia, Catal. Rev. Sci. Eng., 46 (2004) 53–110.

16. Bingfei Cao, Gabriel M. Veith, Joerg C. Neuefeind, Radoslav R. Adzic, and Peter G. Khalifah, J. Am. Chem. Soc., 2013 (135) 19186–19192.

17. Li-Q. Mai, F. Yang, Y. L. Zhao, X. Xu, L. Xu and Y. Z. Luo, Nat. Commun., 2 (2011) 381–385.

18. Y. Ding, Y. Wan, Y. –L. Min, W. Zhang and S.-H. Yu, Inorg. Chem.*,* 47 (2008) 7813–7823.

19. S. C. Verma, B. K. Verma and H. B. Lal, J. Mater. Sci. Lett., 2 (1983) 747–749.

20. X. Xia, W. Lei, Q. Hao, W. Wang and X. Wang, Electrochim. Acta, 99 (2013) 253–261.

21. D. Guo, H. Zhang, X. Yu, M. Zhang, P. Zhang, Q. Li and T. Wang, J. Mater. Chem. A, 1 (2013) 7247–7254.

22. M.-C. Liu, L.-B. Kong, C. Lu, X.-M. Li, Y.- C. Luo and L. Kan, Mater. Lett., 94 (2013) 197–200.

23. X. Xu, J. Shen, N. Li, and M. Ye, J. Alloy. Compd., 616 (2014) 58–65.

24. G. K. Veerasubramani, K. Krishnamoorthy, S. Radhakrishnan, N.-J. Kim, and S. J. Kim, Int. J. Hyd. Energy, 39 (2014) 5186–5193.

25. M. Mandal, D. Ghosh, S. Giri, I. Shakir and C. K. Das, RSC Adv., 4 (2014) 30832–30839.

26. H. Wan, J. Jiang, X. Ji, L. Miao, Li Zhang, K. Xu, H. Chen, and Y. Ruan, Mater. Lett., 108 (2013) 164–167.

27. Q. Zhang, Y. Deng, Z. Hu, Y. Liu, M. Yao and P. Liu, Phys. Chem. Chem. Phys., 16 (2014) 23451–23460.

28. D. Ghosh, S. Giri, Md. Moniruzzaman, T. Basu, M. Mandal and C. K. Das, Dalton Trans., 43 (2014) 11067–11076.

29. Y. Ding, Y. Wan, Y. L. Min, W. Zhang, S. H. Yu, Inorg. Chem., 47 (2008) 7813–7823.

30. J. Chojnacki and R. Kozlowski, J. Solid State Chem., 14 (1975) 117–121

31. V. Blanco-Gutierrez, A. Demourgues and M. Gaudon, Dalton Trans., 42 (2013) 13622–13627.

32. D. Vie, E. Martinez, F. Sapina, J. V. Folgado and A. Beltran, Chem. Mater., 16 (2004) 1697–1703.

33. L. Dambies, T. Vincent, A. Domard and E. Guibal, Biomacromolecules, 2 (2001) 1198–1205.

34. R. A. A. Muzzarelli (Ed.), Natural Chelating Polymers, Pergamon Press, New York (1973), p. 83, J. P. Zikakis (Ed.), Chitin, Chitosan and Related Enzymes, Academic Press, Orlando (1984), p. XVII.

35. S. M. Nomanbhay and K. Palanisamy, Electronic J. Biotech., 8 (2005) 43–53

36. M. N. V. Ravi Kumar, React. Funct. Polym., 46 (2000) 1–27.

37. L. Verestiuc, O. Nastasescu, E. Barbu, I. Sarvaiya, K. L. Green and J. J. Tsibouklis, J Biomed. Mater. Res. A, 77 (2006) 726–735.

38. M. Selvakumar and D. Krishna Bhat, J. Appl. Polym. Sci., 114 (2009) 2445–2454.

39. N. A. Choudhury, P. W. C. Northrop, A. C. Crothers, S. Jain and V. R. Subramanian, J. Appl. Electrochem., 42 (2012) 935–943.

40. S. Hassan, M. Suzuki, and A. A. El-Moneim, J. Power Sources, 246 (2014) 68–73.

41. K. Pandiselvi and S. Thambidurai, Ionics, 20 (2014) 551–561.

42. B. Senthilkumar, D. Meyrick, R. Kalaiselvan, and M. Minakshi, Chem. Engg. J., 253 (2013) 502–507.

43. R. B. Iglesias, R. Coronilla, A. Concheiro and C. A. Lorenzo, Eur. J. Pharm. Sci., 24 (2005) 77–84.

44. K.-S. Park, S.-D. Seo, H.-W. Shim and D.-W. Kim, Nanoscale Research Lett., 7 (2012) 1–7.

45. B. Li, C.-L. Shan, Q. Zhou, Y. Fang, Y.-L. Wang, F. Xu, L.-R. Han, M. Ibrahim, L.-B. Guo, G.-L. Xie and G.-C. Sun, Mar. Drugs, 11 (2013), 11, 1534-1552.

46. M. Hasegawa, A. Isogai and F. Onabe, Carbohydr. Polym., 20 (1993) 279–283.

47. T. Mitra, G. Sailakshmi, A. Gnanamani, A. B. Mandal, J. Mater. Sci., 23 (2012) 1309–1321.

48. M. Jabli, M. H. V. Baouab, N. Sintes-Zydowicz, B. B. Hassine, J. Appl. Polym. Sci., 123 (2012) 3412–3424.

49. S. T. Aruna and A. S. Mukasyan, Curr. Opin. Solid State Mater. Sci., 12 (2008) 44–50.

50. S. J. Pennycook, A. R. Lupini, M. Varela, A. Y. Borisevich, Y. Peng, M. P. Oxley and M. F. Chisholm, "*Scanning Transmission Electron Microscopy for Nanostructure Characterization*," pp. 152-191 in *Scanning Microscopy for Nanotechnology: Techniques and Applications*, ed. by W. Zhou and Z. L. Wang, Springer 2006.

51. Z. Xu, Z. Li, X. Tan, C. M. B. Holt, L. Zhang, B. C. Amirkhiz, D. Mitlin, RSC Adv., 2 (2012) 2753–2755.

52. D. Ghosh, S. Giri, A. Mandal and C. K. Das, RSC Adv., 3 (2013) 11067–11076.

53. R. A. Zangmeister, J. J. Park, G. W. Rubloff and M. J. Tarlov, Electrochim. Acta, 51 (2006) 5324–5333.

54. Y. Kawamura, M. Mitsuhashi, H. Tanibe, Ind. Eng. Chem. Res., 32 (1993) 386−391.

55. M. D. Levi and D. Aurbach, J. Phy. Chem. B, 101 (1997) 4641–4647.

56. M.-C. Liu, L.-B. Kong, X.-J. Ma, C. Lu, X.-M. Li, Y.- C. Luo and L. Kan, New J. Chem. 36 (2012) 1713 – 1716.

57. B. Senthilkumar, R. Kalaiselvan, D. Meyrick and M. Minakshi, Int. J. Electrochem. Soc. 10 (2015) 185 – 193.

58. M. Minakshi, S. Baskar, M. Ionescu and D. Khushalani (2015) Unpublished work.
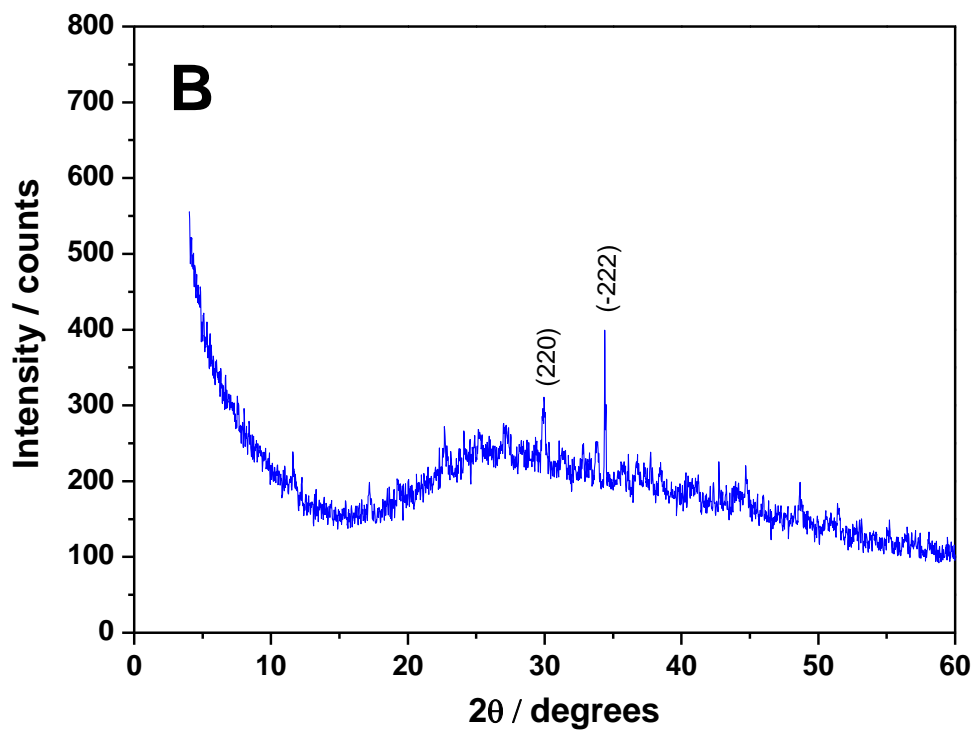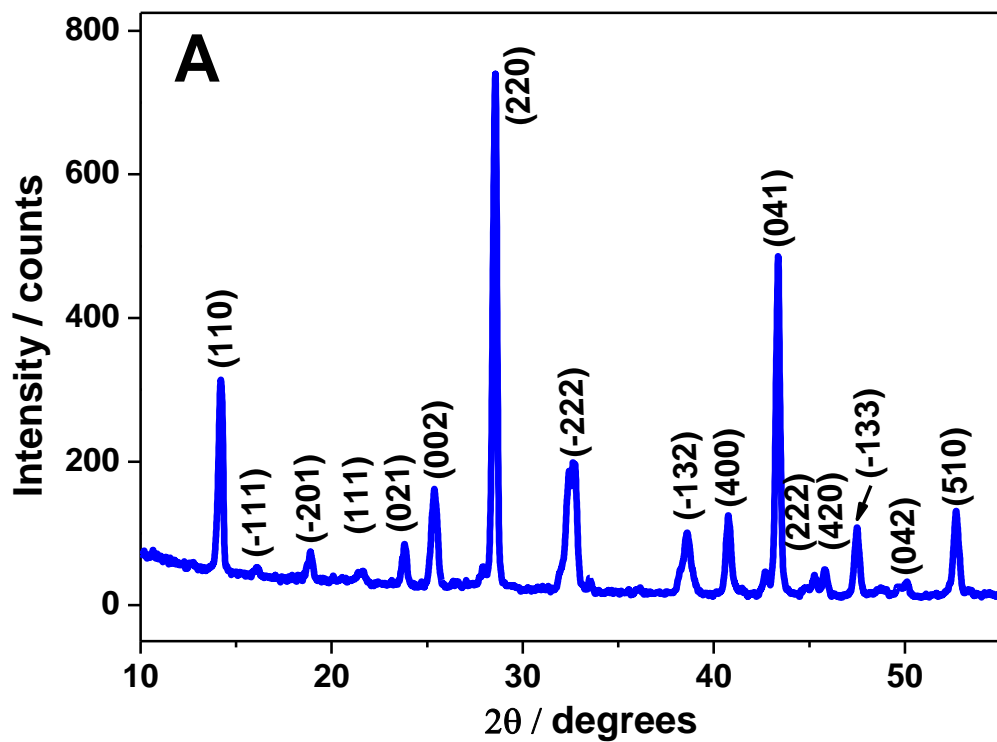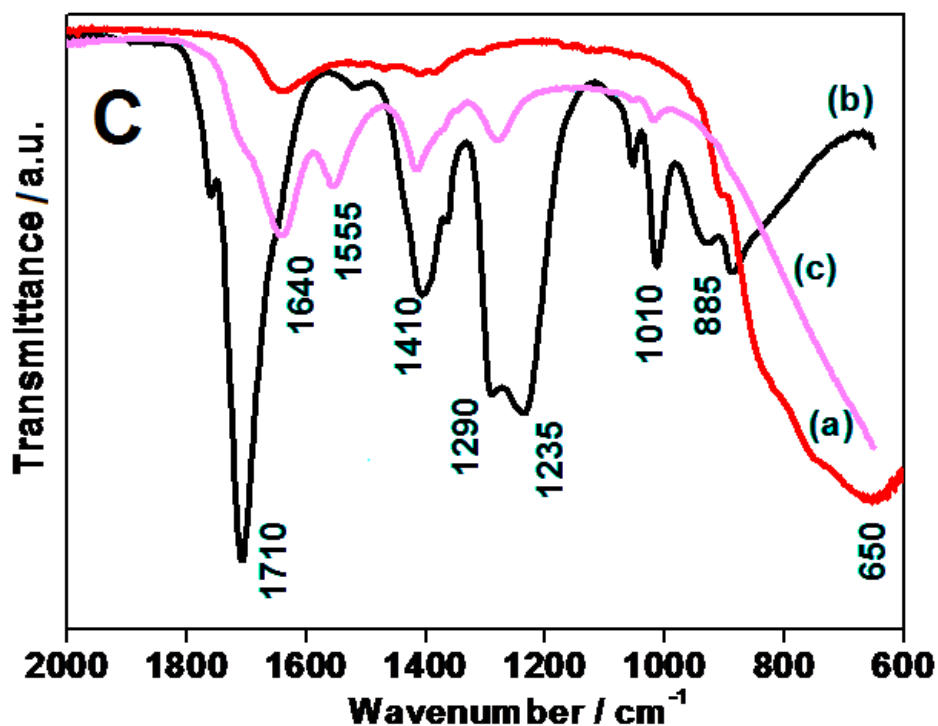
Figure 1 X-ray diffraction (XRD) patterns of $CoMoO_4$ (A) and $CoMoO_4$ modified with chitosan (B). Infrared spectra of $CoMoO_4$ (C) showing (a) as-prepared $CoMoO_4$ (b) chitosan dissolved in acetic acid and (c) chitosan dissolved in acetic acid then reacted with glutaraldehyde and to the resultant gel, $CoMoO_4$ powder was added.
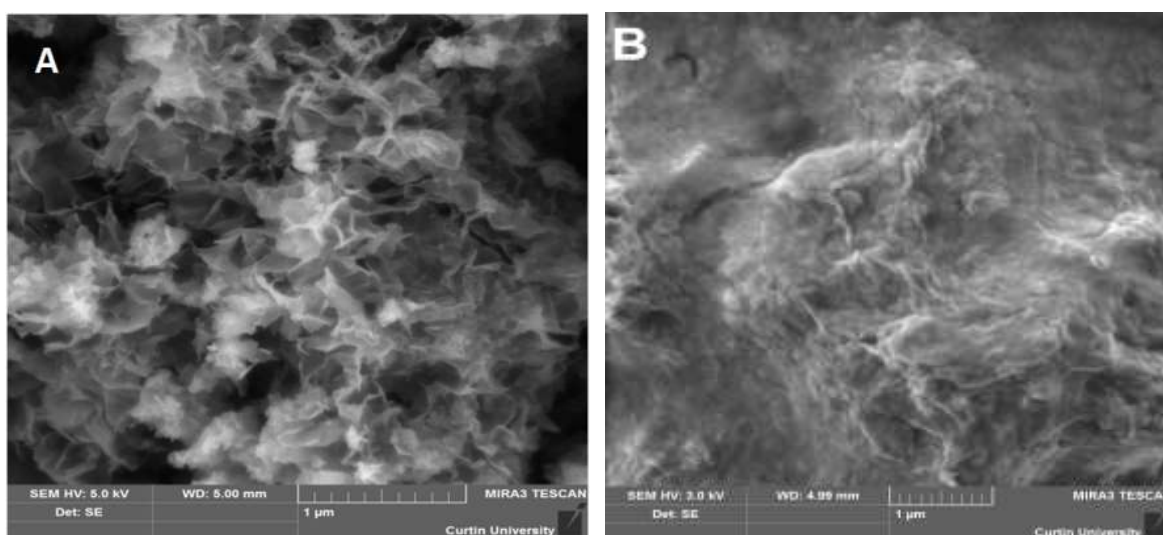
Figure 2 FIB-SEM images of $CoMoO_4$ (A) and $CoMoO_4$ modified with chitosan (B).
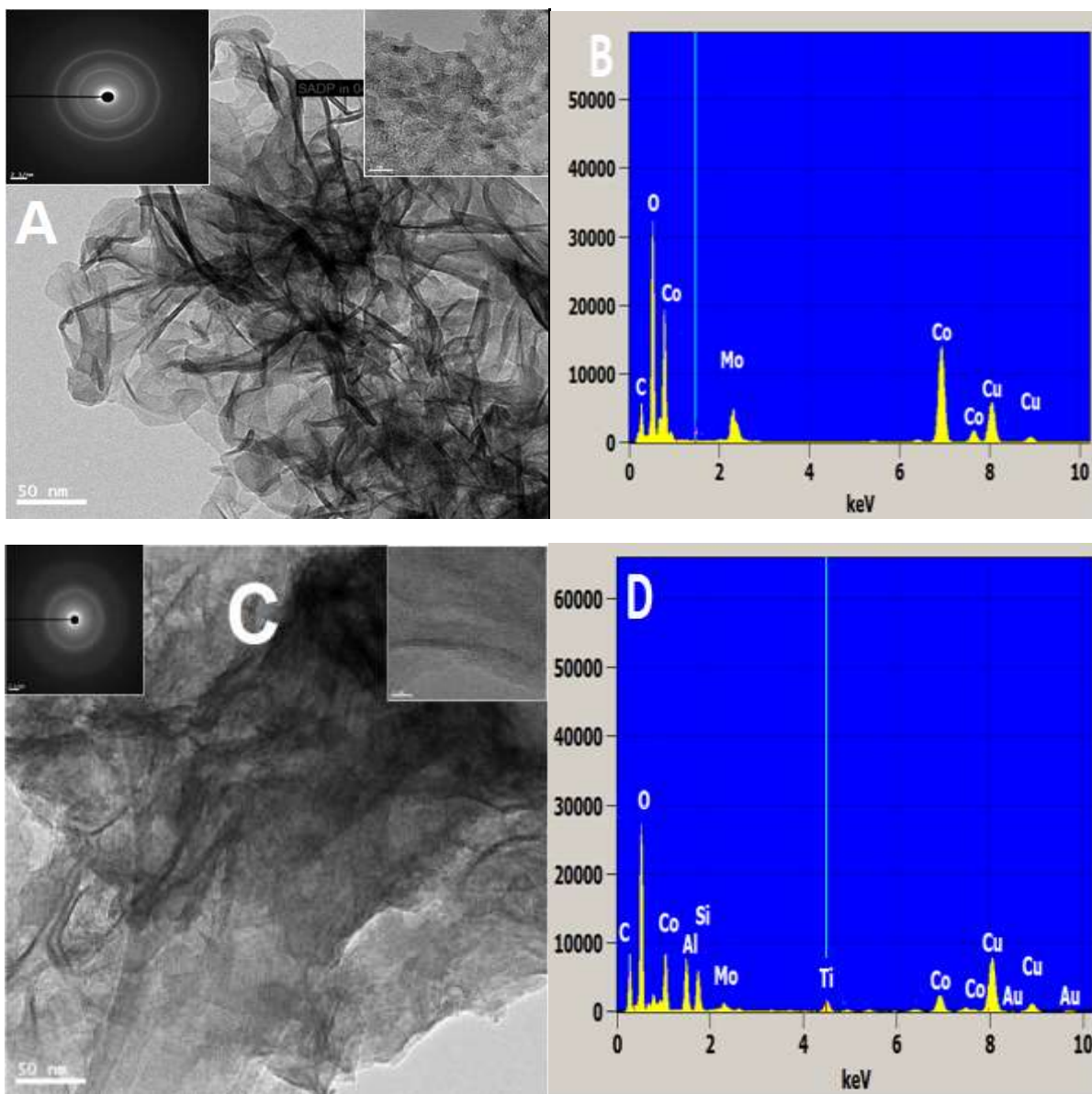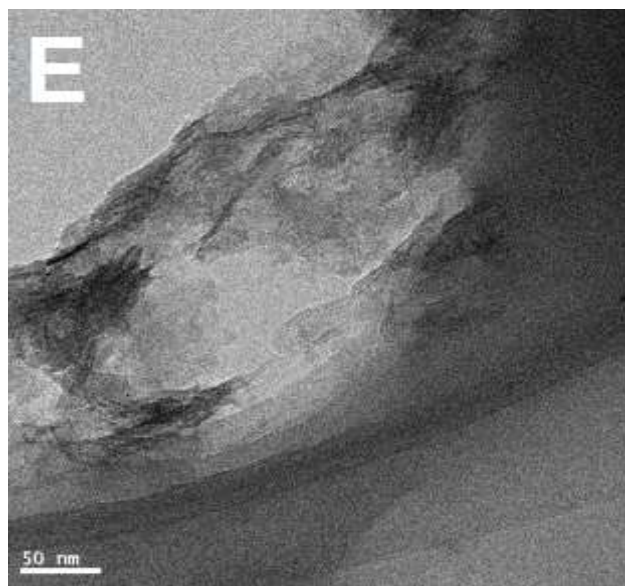
Figure 3 TEM images and corresponding EDS spectra of $CoMoO_4$ (A and B) and $CoMoO_4$ modified with chitosan (C and D). SADP and HR-TEM were shown in the left and right insets of the respective images. Another region (E) showing an interface between the $CoMoO_4$ and the organic particles enhancing the adsorption.
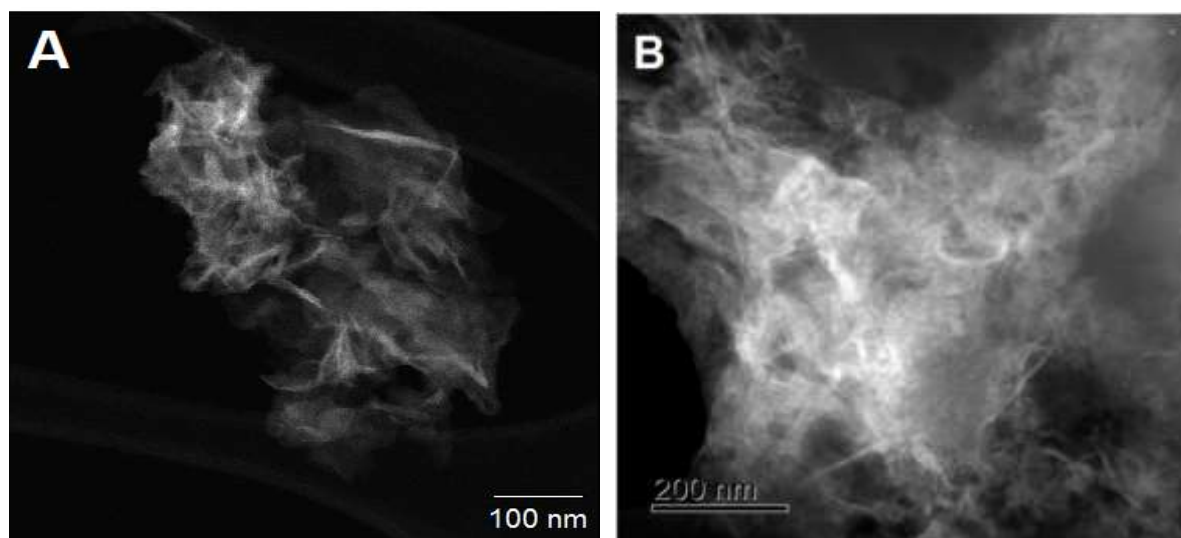
Figure 4 Comparison of raw STEM images showing CoMoO$_4$ (A) and CoMoO$_4$ modified with chitosan (B) nanoparticles in few nm and interestingly the particle size is further reduced for modified samples (to be noted scales are different), enabling the storage capability.
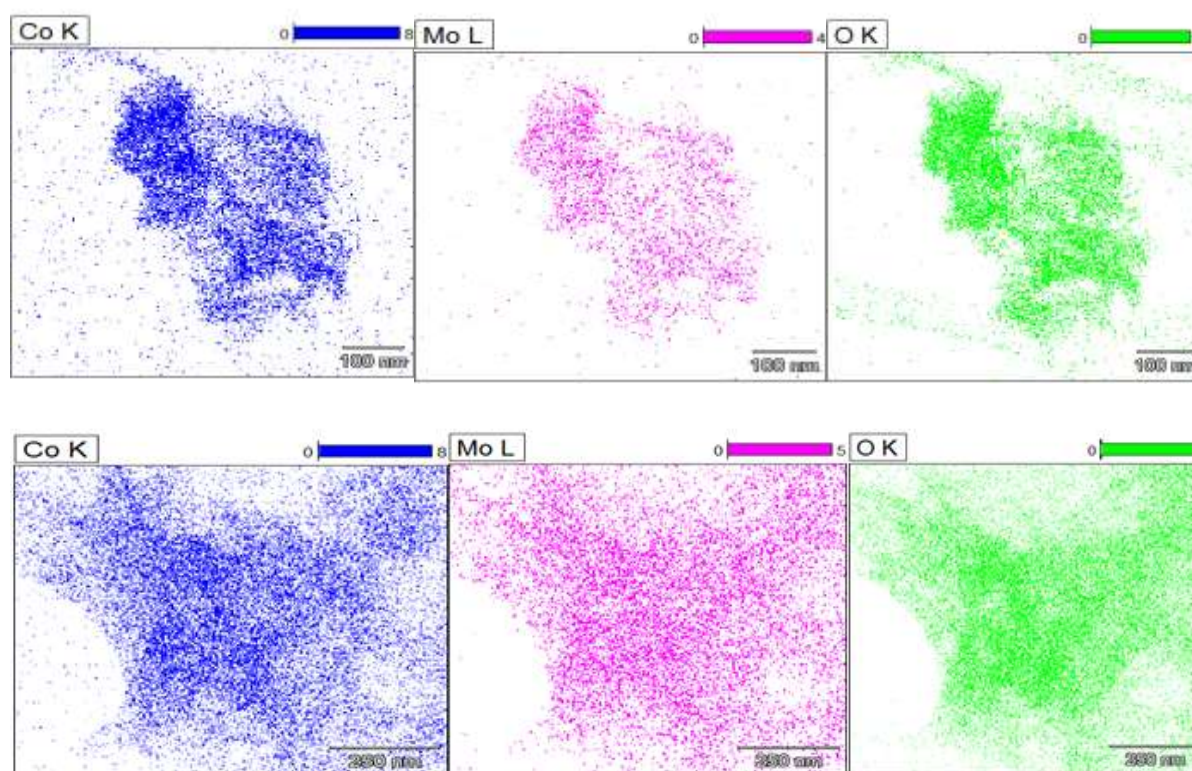
Figure 5 Composition profiles of CoMoO$_4$ (4A) and CoMoO$_4$ modified with chitosan (4B) nanoparticles showing the individual elements Co, Mo and O regions.
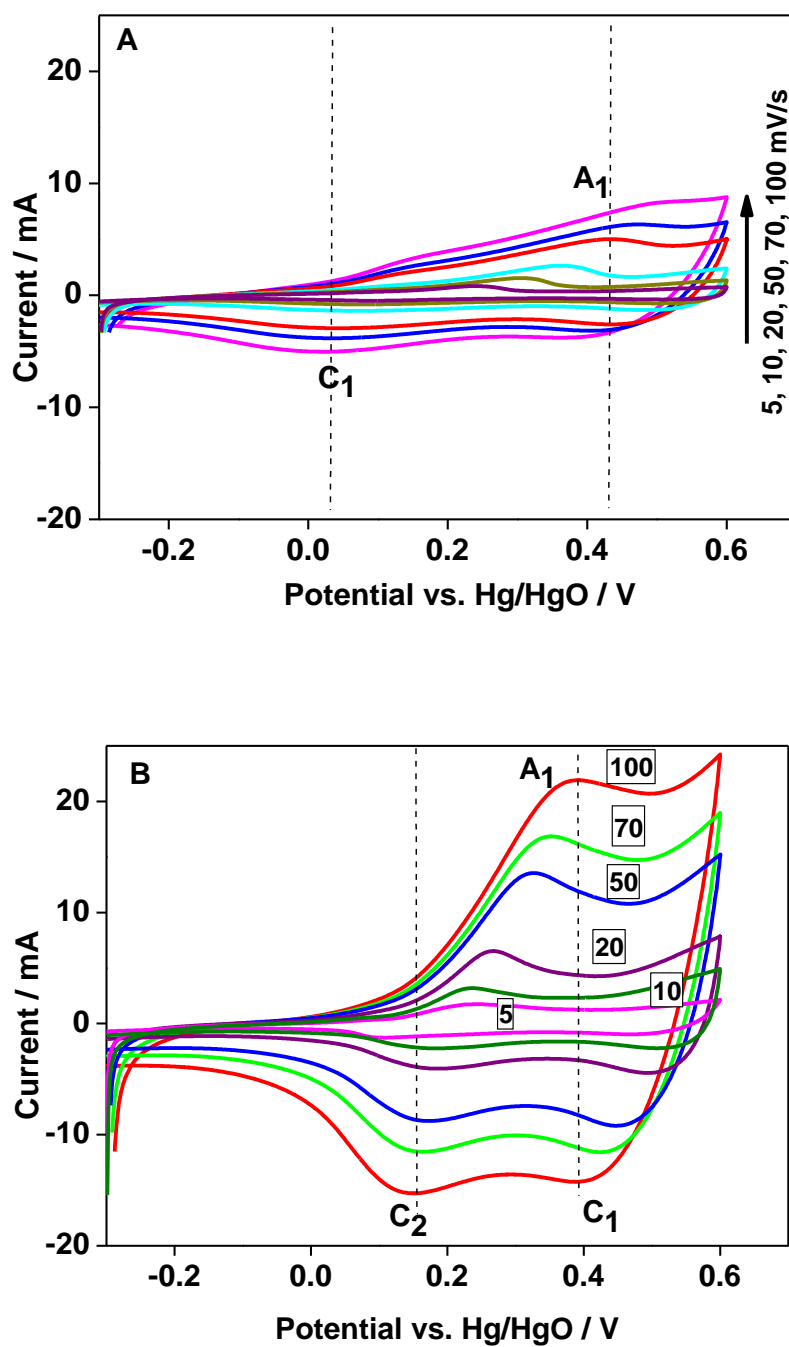
Figure 6 Cyclic voltammetric curves (three-cell configuration) of the CoMoO$_4$ (A) and CoMoO$_4$ modified with chitosan (B) at scan rates indicated in the figure in 2M aqueous NaOH electrolyte. A platinum wire is used as a counter electrode.

26
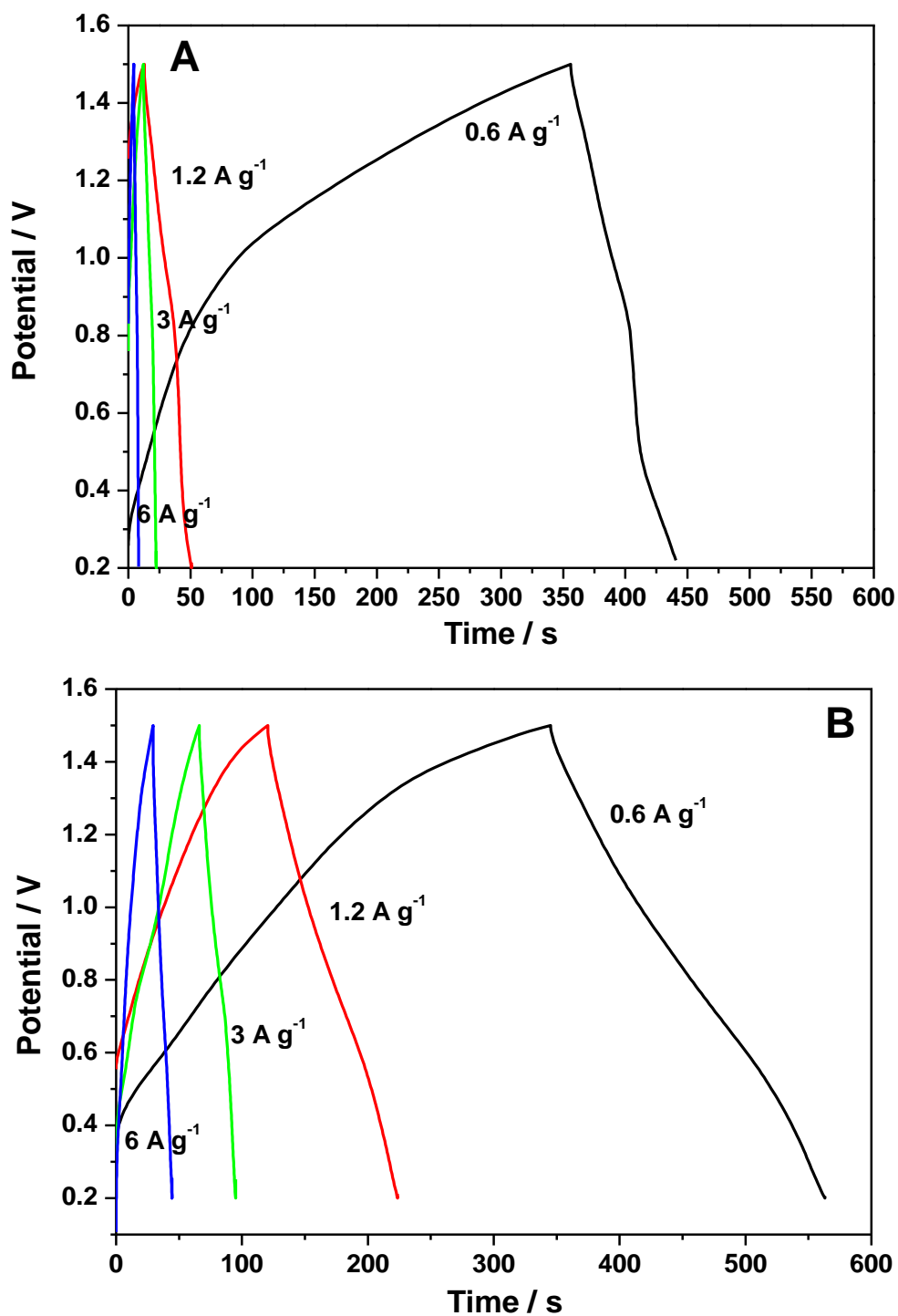
Figure 7 Galvanostatic charge-discharge curves of the CoMoO$_4$ *vs*. AC (A) and modified CoMoO$_4$ with chitosan *vs*. AC (B) at current densities indicated in the figure in 2M aqueous NaOH electrolyte
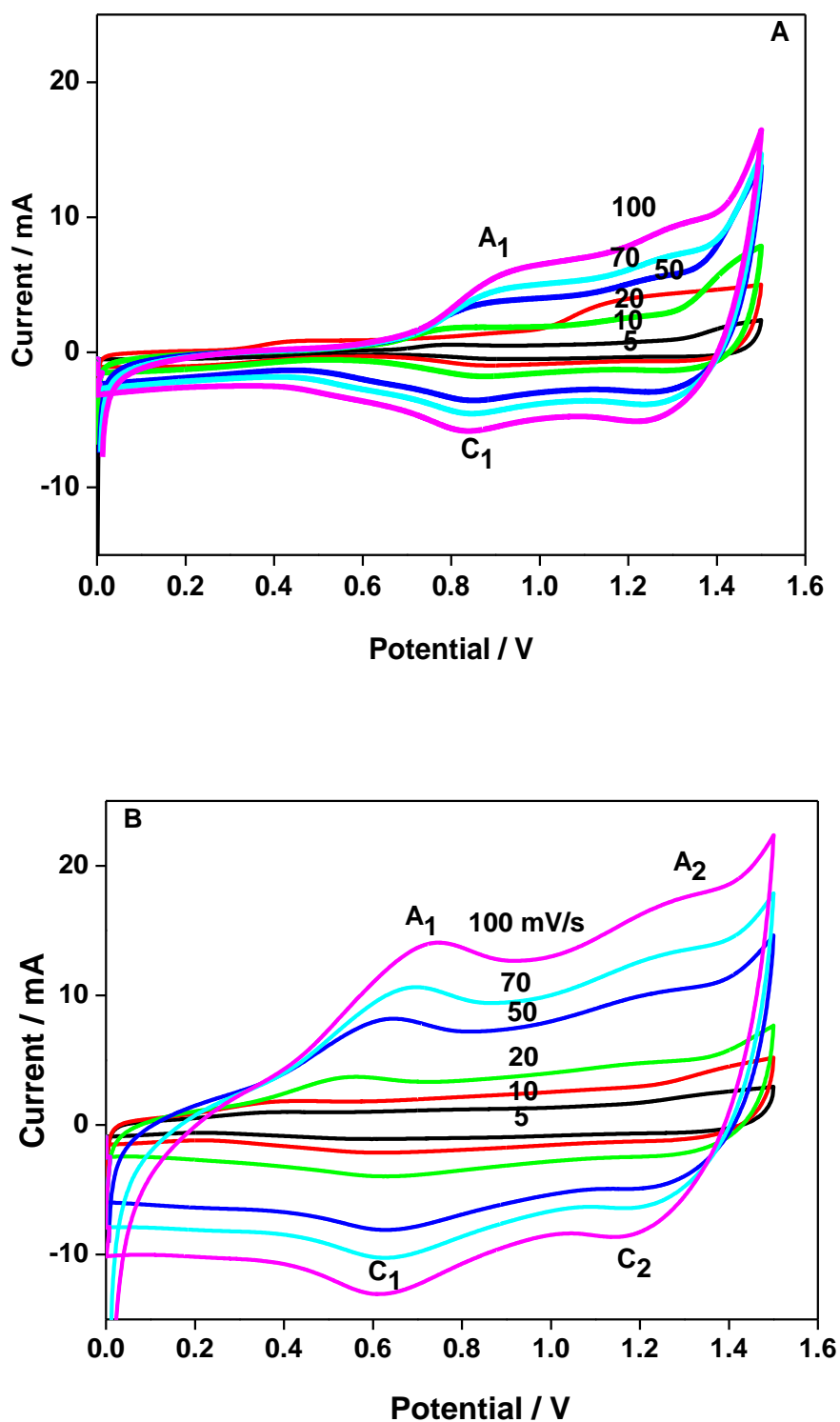
Figure 8 Cyclic voltammetric curves (two-cell configuration) of the CoMoO$_4$ *vs*. AC (A) and CoMoO$_4$ modified with chitosan *vs*. AC (B) at scan rates indicated in the figure in 2M aqueous NaOH electrolyte. Reported potential is with respect to activated carbon.

Dalton Transactions
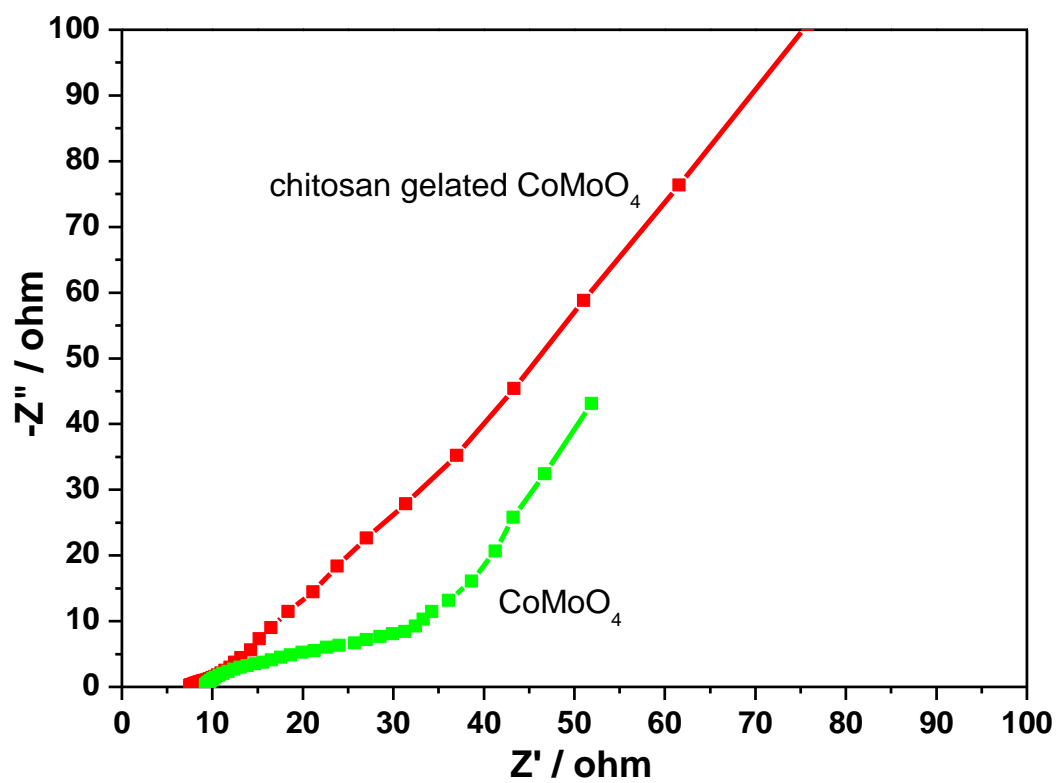
Figure 9 Nyquist impedance spectra for the cycled CoMoO$_4$ (A) and modified CoMoO$_4$ with chitosan (B)
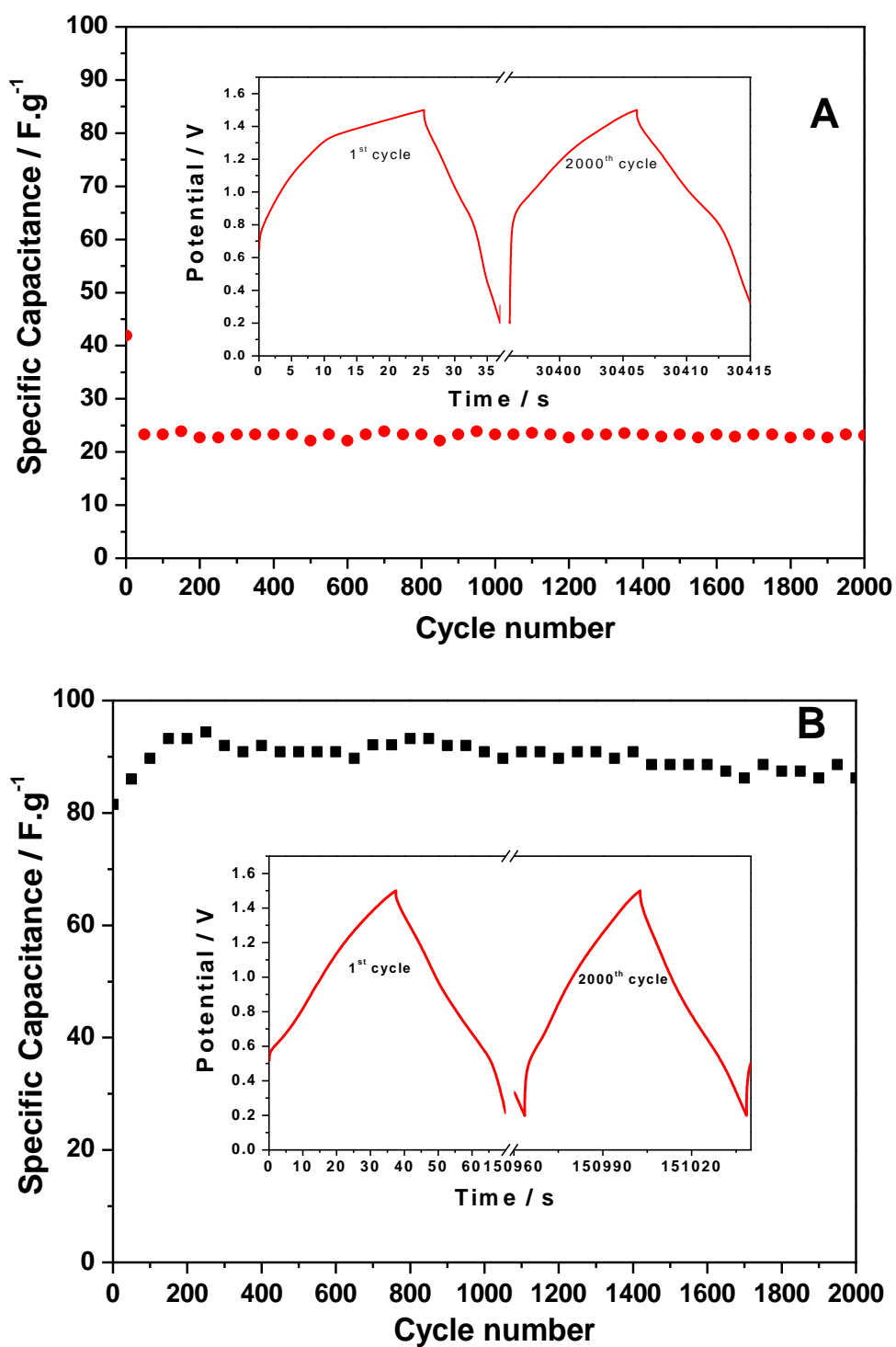
Figure 10 Variation of the specific capacitance *vs*. the cycle number at a rate of 3 A/g for the CoMoO$_4$ (A) and modified CoMoO$_4$ with chitosan (B).
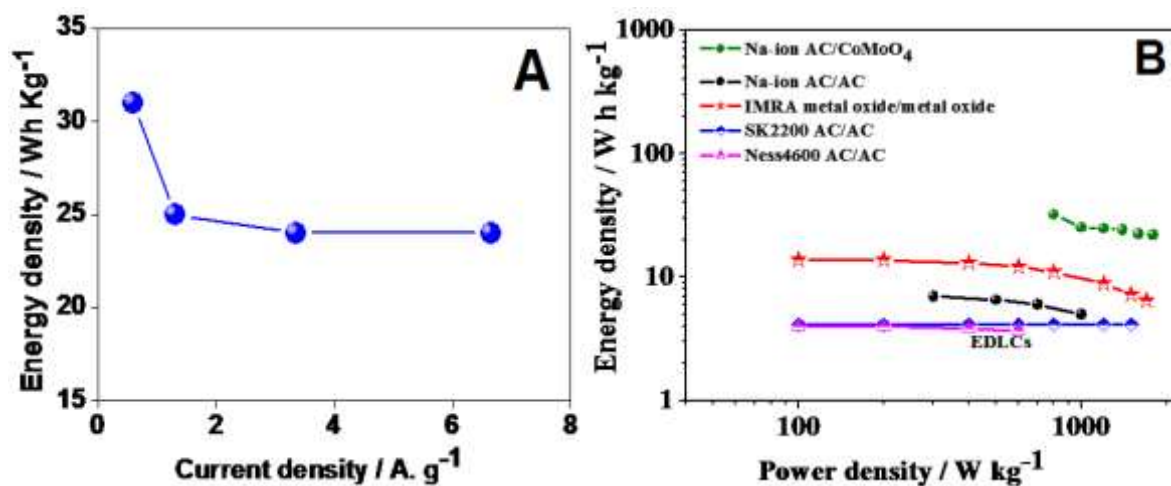
Figure 11 Plot of energy density *vs.* current density for the modified $CoMoO_4$ with chitosan (A) and Ragone plot for various energy storage devices compared with modified $CoMoO_4$ with chitosan (B). Fig. 11 (b) is reproduced from ref [58].

Table 1 Specific capacitance of $CoMoO_4$ materials obtained through galvanostatic charge-discharge studies at different current densities

Current Density (mA/cm^2)	Specific Capacitance of as-prepared $CoMoO_4$ (F/g)	Specific Capacitance of $CoMoO_4$ modified with chitosan (F/g)
1	46	135
2	23	110
5	29	105
10	28	105
5 (after 2000 cycles)	17	81

Table 2 Specific capacitance of CoMoO$_4$ materials obtained through potentiodynamic method at different sweep rates

Scan rate (mV/s)	Specific Capacitance of as-prepared CoMoO$_4$ (F/g)	Specific Capacitance of CoMoO$_4$ modified with chitosan (F/g)
5	56	179
10	54	164
20	58	135
50	42	108
70	36	94
100	32	82